Quantum Rod-Sensitized Solar Cell: Nanocrystal Shape Effect on the Photovoltaic Properties

ARTICLE *in* NANO LETTERS · MARCH 2012

Impact Factor: 13.59 · DOI: 10.1021/nl300356e · Source: PubMed

6 AUTHORS, INCLUDING:

Menny Shalom
Max Planck Institute of Colloids and Interfaces
37 PUBLICATIONS **1,878** CITATIONS
SEE PROFILE

Zion Tachan
Bar Ilan University
13 PUBLICATIONS **596** CITATIONS
SEE PROFILE

Arie Zaban
Bar Ilan University
170 PUBLICATIONS **10,728** CITATIONS
SEE PROFILE

NANO LETTERS

Letter

pubs.acs.org/NanoLett

Quantum Rod-Sensitized Solar Cell: Nanocrystal Shape Effect on the Photovoltaic Properties

Asaf Salant,[†,§] Menny Shalom,[‡,§] Zion Tachan,[‡] Sophia Buhbut,[‡] Arie Zaban,*[,‡] and Uri Banin*[,†]

[†]Institute of Chemistry and the Center for Nanoscience and Nanotechnology, The Hebrew University, Jerusalem 91904, Israel

[‡]Department of Chemistry, Bar-Ilan University, 52900 Ramat-Gan, Israel

Supporting Information

ABSTRACT: The effect of the shape of nanocrystal sensitizers in photoelectrochemical cells is reported. CdSe quantum rods of different dimensions were effectively deposited rapidly by electrophoresis onto mesoporous TiO_2 electrodes and compared with quantum dots. Photovoltaic efficiency values of up to 2.7% were measured for the QRSSC, notably high values for TiO_2 solar cells with ex situ synthesized nanoparticle sensitizers. The quantum rod-based solar cells exhibit a red shift of the electron injection onset and charge recombination is significantly suppressed compared to dot sensitizers. The improved photoelectrochemical characteristics of the quantum rods over the dots as sensitizers is assigned to the elongated shape, allowing the build-up of a dipole moment along the rod that leads to a downward shift of the TiO_2 energy bands relative to the quantum rods, leading to improved charge injection.

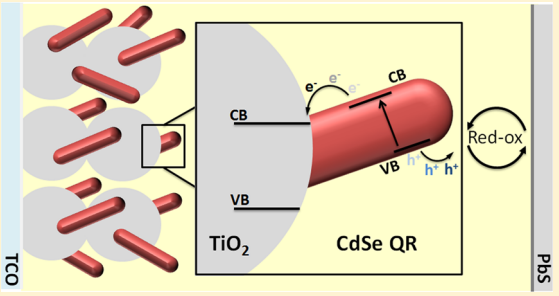

KEYWORDS: *Quantum rods, quantum particle sensitized solar cells, quantum dots, photovoltage spectroscopy, transient photovoltage*

Quantum particle sensitized solar cells (QPSSCs) represent an interesting approach for potentially low cost solar cells[1−3] extending upon the concepts of thin layer semiconductor polycrystalline based solar cells[4−6] and the dye sensitized solar cell[7] architectures. Different designs of QPSSCs have been developed reaching efficiencies of more than 5%.[8−10] In a QPSSC, semiconductor nanoparticles (NPs) such as quantum dots (QDs) are used as sensitizers to absorb solar light and inject electrons into a wide band gap semiconductor, usually mesoporous TiO_2, facilitating charge separation. In an ensuing step, the holes are removed by a redox couple electrolyte that is in contact with the NPs and a cathode. Two main preparation methods are known for QPSSCs. The first is in situ growth, where the NPs are synthesized inside the mesoporous TiO_2.[9,11−18] Having the advantage of forming good heterojunctions between the NPs and the semiconductor electrode, the in situ growth has a drawback of limited control over the size, size distribution, and the morphology of the in situ grown NPs. The second method is the ex situ approach, where the NPs are first synthesized and purified, and next deposited into the mesoporous TiO_2 using various methods.[19−23] This benefits from the continuous developments of synthetic routes facilitating preparation of NPs with controllable sizes,[24] diverse morphologies,[25−27] and new compositions,[28] leading to new characteristics.[29,30] These NPs may have advantages as sensitizers in solar cells due to the ability to tune their electrical and optical properties leading to improved efficiencies.[31−35] Here we study the utilization of quantum rods as sensitizers in a quantum rod sensitized solar cell (QRSSC), demonstrate the effective loading of mesoporous electrodes with QRs using electrophoretic deposition, and probe the effect of sensitizer shape on the physicochemical properties and the cell characteristics.

QRs, manifesting the transition from zero-dimensional (0D) quantum dots to one-dimensional (1D) quantum wires, are interesting candidates to be used as sensitizers in solar cells. The additional dimension of rod length compared to just diameter control in QDs, adds a further knob to tune the particle characteristics, while commonly the diameter of rods still remains the dominant factor for tuning the spectrum via quantum confinement.[36] Previous work on hybrid nanoparticle−polymer solar cells, reported that QRs exhibited improved characteristics compared with QDs.[37−41] We study the use of QRs as sensitizers in the QRSSC considering that they may improve the cell characteristics due to several reasons: QRs volumes are larger than QDs and therefore they have significantly larger per-particle absorbance cross sections.[42] This is expected to increase the optical density of electrodes covered by up to a single layer of NP sensitizers and therefore improve light harvesting. In addition, hole and electron wave functions may be more easily separated throughout the QRs,[43−45] facilitating easier electron−hole charge separation that may increase electron injection efficiency from QRs. Furthermore, the surface area of QRs on a per particle basis is larger compared to QDs, which may allow larger contact area and hence improve the interfacial contact between them and the

Received: January 27, 2012
Revised: March 17, 2012
Published: March 27, 2012

surrounding electrolyte. This can further improve charge separation efficiency leading to higher performance of the QRSSC.

A challenge for the realization of a QRSSC is related to difficulties in effective loading and penetration of the relatively large QRs into the depth of the mesoporous electrode. Electrophoretic deposition (EPD) of NPs can assemble QDs[46,47] and QRs[48,49] on various substrates, and it has also been tested for solar cell applications.[50−52] However, the effect of the morphology of the sensitizer on the solar cell performance was not examined. Recently we demonstrated the facile fabrication of QDSSCs based on deposition of QDs into mesoporous wide band gap semiconductor electrodes using EPD,[23] without the need of functionalization of the electrode surface with organic linkers. The QDs penetrated into the TiO_2 layer rapidly and effectively leading to improved photovoltaic (PV) properties in comparison to previous reports.

In this research, we demonstrate and study the utilization of quantum rods as sensitizers in photo electrochemical solar cells prepared by the EPD technique. The dependence of the QRSSCs performance on the QRs dimensions is studied for a series of QRs of similar diameters and different lengths and also compared to spherical QDs. The best cell, based on 40 × 5 nm QR, exhibits J_{sc} of 9.7 mA/cm^2, V_{oc} of 564 mV, fill factor of 49%, and a total efficiency of 2.7%. Absorption measurements of the cells indicate that the optical densities of electrodes with short QRs deposited were as high as 1.2 at the exciton peak, while longer QRs exhibit optical densities of ∼0.6, which may be due to a limitation imposed by the pore sizes of the mesoporous TiO_2. Photovoltage spectroscopy (PVS) reveals that the onset of electron injection from the QR into the TiO_2 occurs at longer wavelengths compared to the QDs. This shift for the QRs indicates that the energy band alignment between the QR/TiO_2 is more favorable for electron injection compared with that of the QD/TiO_2. Advanced characterization, utilizing charge extraction measurements, shows that the band alignment results from a positive shift of the TiO_2 with respect to both the CdSe and the electrolyte. Lastly, transient photovoltage measurements show that the rate of recombination from the mesoporous TiO_2 to the electrolyte is significantly reduced for QRSSCs compared to the QDSSC. We assign both the TiO_2 band shift and the reduced recombination associated with the QRs to an electric field formed along the QR by the interfacial asymmetry. Our results indicate the potential advantages of QRs over QDs as sensitizers in photo electrochemical cells.

The effect of sensitizer shape on the loading concentration and the PV properties of the solar cell were studied. To this end, CdSe QRs were synthesized by the hot injection method as previously reported.[25,53,54] Briefly, precursor solutions containing dimethylcadmium and Se were rapidly injected into a hot solution of coordinating ligands that consisted of a mixture of trioctylphosphine oxide and *n*-tetradecylphosphonic acid yielding QRs with controlled lengths and diameters in the dimensions of 17 × 4.8, 30 × 4.8, and 40 × 5.0 nm. QDs of 5.0 nm were also synthesized for comparison (see methods and materials in Supporting Information for details). These dimensions were chosen such that the NPs will have similar absorbance spectra and onsets, by tailoring the bandgaps for the QRs and the QD[36] (Figure S1 and S2 in the Supporting Information).

For deposition onto the mesoporous electrodes, the NPs were cleaned from excess organic ligands by precipitating with acetone and redispersing in toluene, with concentration in the order of ∼1 μM. Fifteen micrometers thick TiO_2 mesoporous electrodes were fabricated using the doctor blade technique and sintered prior to their use. Two counter electrodes were immersed in the NPs solution and a DC voltage of 0.2 kV was applied, allowing the QRs or QDs to be deposited into the TiO_2 electrodes using EPD. The deposition time of the QRs was ∼15 min after which we did not notice further change in optical density. The QRs deposition time is faster than that of the QDs, which lasted ∼2 h. This may be because the QRs have larger surface area per particle, as compared to the QDs, and hence have more ligands that contribute to a larger number of charges per particle.

The absorbance spectra of the sensitized electrodes (Figure 1 and Figures S1,2 in the Supporting Information) show similar

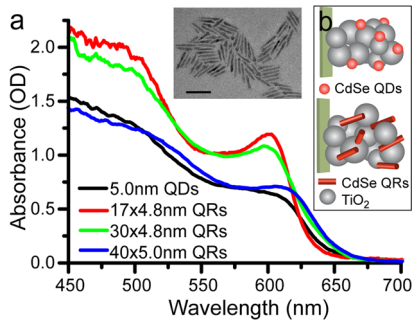

Figure 1. (a) Absorption spectra of mesoporous TiO_2 electrodes sensitized by CdSe NPs. 5.0 nm QDs (black), 17 × 4.8 nm (red), 30 × 4.8 nm (green), and 40 × 5.0 nm QRs (blue). (Inset) TEM image of the 40 × 5.0 nm CdSe QRs, 50 nm scale bar. (b) Illustration of the quantum dot sensitized solar cells (top) and the quantum rod sensitized solar cells (bottom).

optical densities (ODs), measured at the first exciton peak, for the 40 nm QRs (for simplicity, the QRs are referred to by their lengths), (0.69, blue curve) and for the 5 nm QDs (0.63, black curve), while for the shorter QRs, the 17 (red curve) and 30 nm (green curve), higher ODs were measured, around 1.1−1.2. Using Beer−Lambert's law, the concentration and the number of particles deposited on the electrodes were calculated (Table 1). The absorption coefficient is dependent on the volume of the particle; because QRs have larger per-particle absorption coefficients compared with QDs, the number of particles in the 40 nm electrode is about a tenth of that of the 5 nm QDs.

A comparison was made between the EPD and the linker based deposition method[22,55] for the 40 × 5 nm QRs. In the linker approach, the electrode surface was functionalized by immersion in a solution of 3-mercaptopropionic acid to bind the bilinkers for 24 h. In a second step, the functionalized electrode was immersed for another 24 h in a solution of QRs to bind the rods. The cross sections of the electrodes were analyzed using energy dispersive X-ray spectroscopy with a scanning electron microscope (EDS-SEM). The Cd/Ti ratio versus the TiO_2 electrode cross section depth is presented in Figure 2, showing a dramatic difference. Only in the EPD approach the QRs penetrated throughout the electrode depth, which is in contrast to the linker approach where the QRs hardly penetrated into the mesoporous TiO_2. This significant difference is also visualized by examining the front and back sides of the electrodes, clearly showing coloring by the QRs

dx.doi.org/10.1021/nl300356e | *Nano Lett.* 2012, 12, 2095−2100

Table 1. Summary of the Cell Characteristics for the Different QRs and QD Sensitizers[a]

sample (nm)	OD (first exciton)	no. NPs	norm. no. NPs (%)	V_{oc} (mV)	J_{sc} (mA/cm^2)	FF (%)	η (%)
5.0 QDs	0.63	4.0×10^{14}	100	531	7.81	52	2.14
17 × 4.8 QRs	1.19	1.1×10^{14}	27	576	8.19	56	2.64
30 × 4.8 QRs	1.10	9.3×10^{13}	23	548	7.91	45	1.95
40 × 5.0 QRs	0.69	4.6×10^{13}	12	564	9.68	49	2.69

[a]The number of NPs and normalized number of NPs calculated for each electrode based on the optical densities and the absorbance coefficient of the NPs, and summary of the *I*–*V* properties of the different solar cells measured in Figure 3a.

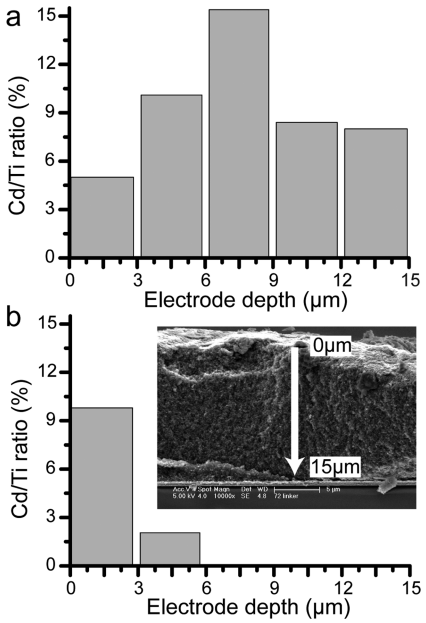

Figure 2. SEM-EDS analysis of cross sections of 15 μm thick TiO_2 mesoporous electrodes loaded with 40 nm CdSe QRs, showing the Cd/Ti ratio as versus the electrode depth, from the top of the electrode toward the FTO covered glass. (a) QRs deposited using EPD, which shows penetration of QRs throughout the mesoporous TiO_2 depth. (b) QRs deposited using the linker approach, showing only partial penetration with a significant concentration of rods only near the outer electrode surface. Inset: SEM image of the cross section for the electrode analyzed prepared using the linker method.

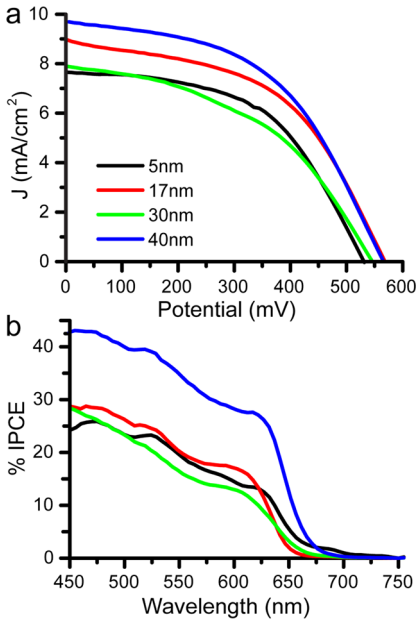

Figure 3. (a) *IV* and (b) IPCE curves of QDs (black) and QRs (17 nm red, 30 nm green, and 40 nm blue) sensitized solar cells. The photovoltaic results are summarized in Table 1. All the cells were larger than 1 cm^2, measured using an illumination intensity of 1 Sun, with an aperture of 1 cm^2.

through the glass side, only for the EPD loaded case (Figure S3 in the Supporting Information). This demonstrates the advantage of the EPD approach in terms of electrode penetration accompanied by the ease of deposition, as the deposition time is vastly shortened compared with the linker approach. In fact, considering the nominal TiO_2 particle size used in the electrode preparation (25 nm), the EPD method is essential for allowing efficient loading of the QRs onto the electrodes.

The electrodes were post treated by ZnS using successive dip coating in aqueous solutions of Zn^{+2} and S^{-2}.[56,57] Previous research showed that ZnS coating significantly enhances the photovoltaic properties by inhibiting recombination.[23,56,57] We note that the wetting angle of the electrode changes after the ZnS treatment from hydrophobic to more hydrophilic (Figure S4 in the Supporting Information). The photovoltaic properties (*IV* curves) and the incident photon to electron conversion efficiency (IPCE) of the ZnS treated electrodes were measured (Figure 3a,b), and the *IV* characteristics are summarized in Table 1. The best solar cell performance was measured for the 40 nm QR electrode, with J_{sc} of 9.68 mA/cm^2, V_{oc} of 564 mV, fill factor of 49%, and an overall efficiency of 2.7%. This efficiency level is among the higher values reported so far for QPSSC using ex situ particle synthesis. While there are only slight differences between the absorbance spectra of the 40 nm QRs and the 5 nm QDs (Figure S5a,b in the Supporting Information), both the *IV* and the IPCE values of the QRs are better than the values measured for the QDs demonstrating the benefits of QRs as sensitizers. Consequently, the following discussion will concentrate on the comparable couple, the 5 nm QD versus the 40 nm QR sensitizers.

To gain further understanding of the sensitizer shape effect on the solar cell performance, we performed advanced characterizations by photovoltage spectroscopy (PVS), charge extraction and transient photovoltage (TPV) measurements. Photovoltage spectroscopy is a sensitive tool which detects the onset of electron injection from the sensitizer into the TiO_2 by measuring V_{oc} as a function of the illumination wavelength.[58] Focusing on the normalized V_{oc} onset of the different electrodes, between 600 and 700 nm (Figure 4, solid lines), reveals that the photovoltage onset of the QRs starts at ~675 nm while for the QDs the onset is at ~640 nm, even though the absorption onsets are shifted by less than 5 nm (Figure 4, dots). Taking into account the small difference in absorption, the PVS results indicate that the band offset between the QR and the TiO_2 conduction band is ~70 meV larger than that of the QD/TiO_2 interface, allowing electron injection at lower

dx.doi.org/10.1021/nl300356e | Nano Lett. 2012, 12, 2095–2100

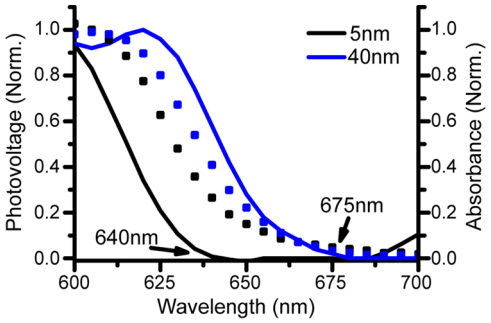

Figure 4. Measurement of the photovoltage (solid lines, left *Y* axis) and absorbance (dots, right *Y*-axis) as a function of the wavelength for 40 nm QRs and the 5 nm QDs (both normalized at the first exciton peak). The onset wavelength at which photovoltage initiates is at higher wavelengths for QRs ~675 nm, compared to the QDs at ~640 nm.

excitation energies. We attribute the band offset to the rod geometry, as will be further discussed.

Further evidence for a shape-induced shift of the band alignment at the NP/TiO_2 interface is provided by charge extraction measurements. Charge extraction is a technique that measures the charge and electron density in the photoactive electrode as a function of the steady state open circuit photovoltage (V_{oc}).[59−62] Figure 5 presents the electron density

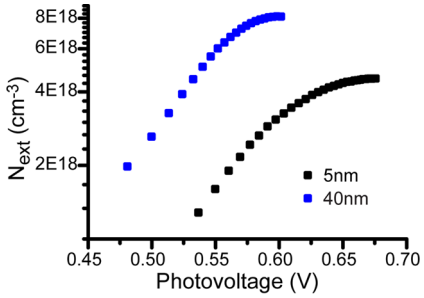

Figure 5. Number of extracted electrons as a function of the photovoltage for the QRSSCs and QDSSC.

in the sensitized electrodes as a function of photovoltage for the cells consisting of the 5 nm QD, and 40 nm QR sensitizers. The similar slopes indicate comparable distribution of states within the two TiO_2 electrodes. Under these conditions, higher electron densities indicate a downward shift of the TiO_2 energy levels toward the redox electrolyte. Consequently, Figure 5 reveals a band shift of the underlying TiO_2 that is modified by the sensitizer shape. The TiO_2 sensitized by the QRs is positioned ~80 mV positive of the QD sensitized analogue, in good agreement with the PVS results (Figure 4).

Energetic shifts of the TiO_2 bands are mostly associated with surface dipoles, molecular layers, ion adsorption, and inorganic coatings.[63,64] Since the sole difference between the QDSSC and QRSSC is the shape of the sensitizer, we attribute the measured bands shift to the ability of the QR to build a dipole moment between two asymmetrical edges along the rod, in contrast to the QDs that are too small to express this asymmetry in energetic terms.[44] The adsorbed QRs are mostly exposed to the polysulfide electrolyte while being connected to the TiO_2 surface at a point along the rod. This is expected to position the CdSe bands which are closer to the polysulfide at a more negative potential compared with the bands that are closer to the CdSe/TiO_2 interface.[65,66] Consequently, the TiO_2 surface is coated with effective dipoles that are spread along the QRs, pushing the TiO_2 bands downward as schematically demonstrated in Figure 6. We note that the CdSe adsorption to the

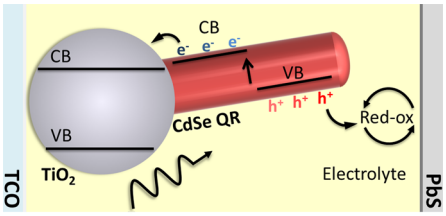

Figure 6. An illustration of the intrinsic charge separation within the QRs.

TiO_2 along the rod, rather than at one of the edges, will affect the dipole magnitude but still maintains the shift direction.

The above understanding of QR-induced surface dipole may explain the significant difference in recombination rates between QRSSCs and QDSSCs. The lifetimes calculated from transient photovoltage (TPV) measurements[67] reveal significantly slower recombination rates for the QRSSC in all cell voltages (Figure 7a). Recombination rates are the product

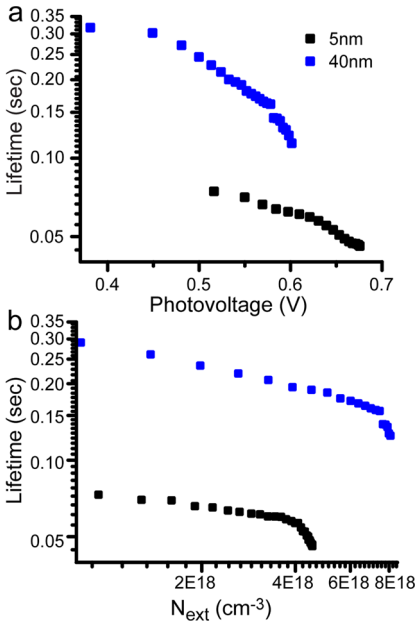

Figure 7. Lifetime decays of excited electrons measured as function of (a) photovoltage and (b) electron density for the 40 nm QRs and 5 nm QDs. QRs based solar cells inhibits recombination processes in the cell, resulting in improved photovoltaic properties.

of the rate constant and the electron concentration in the TiO_2 electrode. Consequently, plotting the electron lifetime as a function of the electron density identifies the observed difference with slower reaction rate constants (Figure 7b). Our understanding of the dipole moment induced in the QRs by the asymmetry of their edges, dictates a slower recombination mechanism attributed to the spatial separation between the TiO_2 surface and the holes extracted to the electrolyte, resulting in slower rate constant for recombination when compared with QDs.

dx.doi.org/10.1021/nl300356e | *Nano Lett.* 2012, 12, 2095−2100

In summary, QRs and QDs sensitized solar cells were fabricated using EPD. The cells were characterized using photo voltage spectroscopy, charge extraction, and transient photovoltage measurements all leading to a common understanding regarding a functional difference between QRs and QDs as sensitizers. The cell geometry in which the CdSe sensitizer is positioned at the TiO_2 electrode/electrolyte interface may induce asymmetry for the QRs that develop a field between the edge connected to the TiO_2 and the edge exposed to the electrolyte, which is in contrast to QDs that are too small to express this asymmetry in energetic terms. Consequently, the TiO_2 bands are shifted positively while hole extraction occurs at a distance from the TiO_2, both leading to higher injection flux and slower recombination. The results show the prospect of shifting from QDs to QRs sensitizers in photoelectrochemical solar cells. The best performance was observed for the 40 × 5 nm QRs based solar cell, reaching 2.7% efficiency at 1 Sun, which is one of the higher efficiencies reported for ex situ QPSSCs. Even though the configuration of the mesoporous-TiO_2 is not optimal for QRs due to the lower coverage, the calculated efficiency per particle was higher for QRs compared to QDs. Therefore, QRs offer new opportunities for the improvement of solar cells based on nanoparticles.

■ ASSOCIATED CONTENT

Supporting Information

NPs synthesis method, experimental setup, additional absorbance measurements, images of the electrodes, and wetting angle measurements are available. This material is available free of charge via the Internet at http://pubs.acs.org.

■ AUTHOR INFORMATION

Corresponding Author

*E-mail: (U.B.) banin@chem.ch.huji.ac.il; (A.Z.) zabana@mail.biu.ac.il.

Author Contributions

§Equally contributed to this paper.

Notes

The authors declare no competing financial interest.

■ ACKNOWLEDGMENTS

We wish to thank Dr. Yafit Fleger, Yorai Amit, and Amit Sitt for their contributions. U.B. acknowledges the support of the Wolfson foundation initiative in alternative energy and the Alfred & Erica Larisch memorial chair in solar energy. A.Z. acknowledges financial support within the Israel science foundation, Bikura program. M.S. thanks the "Converging Technologies" program.

■ REFERENCES

(1) Zaban, A.; Micic, O. I.; Gregg, B. A.; Nozik, A. J. *Langmuir* **1998**, *14* (12), 3153−3156.
(2) Nozik, A. J. *Physica E* **2002**, *14* (1−2), 115−120.
(3) Luther, J. M.; Law, M.; Beard, M. C.; Song, Q.; Reese, M. O.; Ellingson, R. J.; Nozik, A. J. *Nano Lett.* **2008**, *8* (10), 3488−3492.
(4) Hodes, G. *Nature* **1980**, *285* (5759), 29−30.
(5) Hodes, G.; Manassen, J.; Cahen, D. *J. Electrochem. Soc.* **1980**, *127* (3), 544−549.
(6) Nicolau, Y. F. *Appl. Surf. Sci.* **1985**, *22*−*3* (May), 1061−1074.
(7) O'Regan, B.; Gratzel, M. *Nature* **1991**, *353* (6346), 737−740.
(8) Yang, Z.; Chen, C.-Y.; Roy, P.; Chang, H.-T. *Chem. Commun.* **2011**, *47* (34), 9561−9571.
(9) Im, S. H.; Lim, C.-S.; Chang, J. A.; Lee, Y. H.; Maiti, N.; Kim, H.-J.; Nazeeruddin, M. K.; Grätzel, M.; Seok, S. I. *Nano Lett.* **2011**, *11* (11), 4789−4793.
(10) Santra, P. K.; Kamat, P. V. *J. Am. Chem. Soc.* **2012**, *134* (5), 2508−2511.
(11) Plass, R.; Pelet, S.; Krueger, J.; Gratzel, M.; Bach, U. *J. Phys. Chem. B* **2002**, *106* (31), 7578−7580.
(12) Niitsoo, O.; Sarkar, S. K.; Pejoux, C.; Ruhle, S.; Cahen, D.; Hodes, G. *J. Photochem. Photobiol., A* **2006**, *181* (2−3), 306−313.
(13) Shalom, M.; Dor, S.; Ruühle, S.; Grinis, L.; Zaban, A. *J. Phys. Chem. C* **2009**, *113* (9), 3895−3898.
(14) González-Pedro, V.; Xu, X.; Mora-Seró, I. n.; Bisquert, J. *ACS Nano* **2010**, *4* (10), 5783−5790.
(15) Mora-Seró, I. n.; Bisquert, J. *J. Phys. Chem. Lett.* **2010**, *1* (20), 3046−3052.
(16) Ruhle, S.; Shalom, M.; Zaban, A. *ChemPhysChem* **2010**, *11* (11), 2290−2304.
(17) Shalom, M.; Hod, I.; Tachan, Z.; Buhbut, S.; Tirosh, S.; Zaban, A. *Energy Environ. Sci.* **2011**, *4* (5), 1874−1878.
(18) Boix, P. P.; Lee, Y. H.; Fabregat-Santiago, F.; Im, S. H.; Mora-Sero, I.; Bisquert, J.; Seok, S. I. *ACS Nano* **2012**, *6* (1), 873−880.
(19) Yu, P. R.; Zhu, K.; Norman, A. G.; Ferrere, S.; Frank, A. J.; Nozik, A. J. *J. Phys. Chem. B* **2006**, *110* (50), 25451−25454.
(20) Kamat, P. V. *J. Phys. Chem. C* **2008**, *112* (48), 18737−18753.
(21) Iván, M.-S.; Sixto, G.; Thomas, M.; Francisco, F.-S.; Teresa, L.-V.; Roberto, G.; Juan, B. *Nanotechnology* **2008**, *19* (42), 424007.
(22) Guijarro, N.; Lana-Villarreal, T.; Mora-Sero, I.; Bisquert, J.; Gomez, R. *J. Phys. Chem. C* **2009**, *113* (10), 4208−4214.
(23) Salant, A.; Shalom, M.; Hod, I.; Faust, A.; Zaban, A.; Banin, U. *ACS Nano* **2010**, *4* (10), 5962−5968.
(24) Peng, Z. A.; Peng, X. *J. Am. Chem. Soc.* **2002**, *124* (13), 3343−3353.
(25) Peng, X. G.; Manna, L.; Yang, W. D.; Wickham, J.; Scher, E.; Kadavanich, A.; Alivisatos, A. P. *Nature* **2000**, *404* (6773), 59−61.
(26) Kanaras, A. G.; Sönnichsen, C.; Liu, H.; Alivisatos, A. P. *Nano Lett.* **2005**, *5* (11), 2164−2167.
(27) Sitt, A.; Salant, A.; Menagen, G.; Banin, U. *Nano Lett.* **2011**, *11* (5), 2054−2060.
(28) Luther, J. M.; Zheng, H.; Sadtler, B.; Alivisatos, A. P. *J. Am. Chem. Soc.* **2009**, *131* (46), 16851−16857.
(29) Krishnan, R.; Hahn, M. A.; Yu, Z.; Silcox, J.; Fauchet, P. M.; Krauss, T. D. *Phys. Rev. Lett.* **2004**, *92* (21), 216803.
(30) Smyder, J. A.; Krauss, T. D. *Mater. Today* **2011**, *14* (9), 382−387.
(31) Greenham, N. C.; Peng, X.; Alivisatos, A. P. *Phys. Rev. B* **1996**, *54* (24), 17628.
(32) Ginger, D. S.; Greenham, N. C. *Phys. Rev. B* **1999**, *59* (16), 10622.
(33) Sun, B. Q.; Marx, E.; Greenham, N. C. *Nano Lett.* **2003**, *3* (7), 961−963.
(34) Gur, I.; Fromer, N. A.; Chen, C.-P.; Kanaras, A. G.; Alivisatos, A. P. *Nano Lett.* **2006**, *7* (2), 409−414.
(35) Rivest, J. B.; Swisher, S. L.; Fong, L.-K.; Zheng, H.; Alivisatos, A. P. *ACS Nano* **2011**, *5* (5), 3811−3816.
(36) Katz, D.; Wizansky, T.; Millo, O.; Rothenberg, E.; Mokari, T.; Banin, U. *Phys. Rev. Lett.* **2002**, *89* (8), 086801.
(37) Huynh, W. U.; Dittmer, J. J.; Alivisatos, A. P. *Science* **2002**, *295* (5564), 2425−2427.
(38) Huynh, W. U.; Dittmer, J. J.; Libby, W. C.; Whiting, G. L.; Alivisatos, A. P. *Adv. Funct. Mater.* **2003**, *13* (1), 73−79.
(39) Gur, I.; Fromer, N. A.; Geier, M. L.; Alivisatos, A. P. *Science* **2005**, *310* (5747), 462−465.
(40) Sun, B.; Greenham, N. C. *Phys. Chem. Chem. Phys.* **2006**, *8* (30), 3557−3560.
(41) Wu, Y.; Wadia, C.; Ma, W.; Sadtler, B.; Alivisatos, A. P. *Nano Lett.* **2008**, *8* (8), 2551−2555.
(42) Shaviv, E.; Salant, A.; Banin, U. *ChemPhysChem* **2009**, *10* (7), 1028−1031.
(43) Shabaev, A.; Efros, A. L. *Nano Lett.* **2004**, *4* (10), 1821−1825.

(44) Rothenberg, E.; Kazes, M.; Shaviv, E.; Banin, U. *Nano Lett.* **2005**, *5* (8), 1581−1586.
(45) Krahne, R.; Morello, G.; Figuerola, A.; George, C.; Deka, S.; Manna, L. *Phys. Rep.* **2011**, *501* (3−5), 75−221.
(46) Islam, M. A.; Xia, Y. Q.; Telesca, D. A.; Steigerwald, M. L.; Herman, I. P. *Chem. Mater.* **2004**, *16* (1), 49−54.
(47) Jia, S.; Banerjee, S.; Herman, I. P. *J. Phys. Chem. C* **2008**, *112* (1), 162−171.
(48) Ryan, K. M.; Mastroianni, A.; Stancil, K. A.; Liu, H.; Alivisatos, A. P. *Nano Lett.* **2006**, *6* (7), 1479−1482.
(49) Ahmed, S.; Ryan, K. M. *Chem. Commun.* **2009**, No. 42, 6421−6423.
(50) Smith, N. J.; Emmett, K. J.; Rosenthal, S. J. *Appl. Phys. Lett.* **2008**, *93* (4), 043504.
(51) Brown, P.; Kamat, P. V. *J. Am. Chem. Soc.* **2008**, *130* (28), 8890−8891.
(52) Farrow, B.; Kamat, P. V. *J. Am. Chem. Soc.* **2009**, *131* (31), 11124−11131.
(53) Murray, C. B.; Norris, D. J.; Bawendi, M. G. *J. Am. Chem. Soc.* **1993**, *115* (19), 8706−8715.
(54) Peng, X. G.; Wickham, J.; Alivisatos, A. P. *J. Am. Chem. Soc.* **1998**, *120* (21), 5343−5344.
(55) Robel, I.; Subramanian, V.; Kuno, M.; Kamat, P. V. *J. Am. Chem. Soc.* **2006**, *128* (7), 2385−2393.
(56) Shen, Q.; Kobayashi, J.; Diguna, L. J.; Toyoda, T. *J. Appl. Phys.* **2008**, *103* (8), 084304−5.
(57) Guijarro, N.; Campina, J. M.; Shen, Q.; Toyoda, T.; Lana-Villarreal, T.; Gomez, R. *Phys. Chem. Chem. Phys.* **2011**, *13* (25), 12024−12032.
(58) Shalom, M.; Rühle, S.; Hod, I.; Yahav, S.; Zaban, A. *J. Am. Chem. Soc.* **2009**, *131* (29), 9876−9877.
(59) Duffy, N. W.; Peter, L. M.; Rajapakse, R. M. G.; Wijayantha, K. G. U. *Electrochem. Commun.* **2000**, *2* (9), 658−662.
(60) Bailes, M.; Cameron, P. J.; Lobato, K.; Peter, L. M. *J. Phys. Chem. B* **2005**, *109* (32), 15429−15435.
(61) Peter, L. M. *J. Phys. Chem. C* **2007**, *111* (18), 6601−6612.
(62) Sanchez-Diaz, A.; Izquierdo, M.; Filippone, S.; Martin, N.; Palomares, E. *Adv. Funct. Mater.* **2010**, *20* (16), 2695−2700.
(63) Ruhle, S.; Greenshtein, M.; Chen, S. G.; Merson, A.; Pizem, H.; Sukenik, C. S.; Cahen, D.; Zaban, A. *J. Phys. Chem. B* **2005**, *109* (40), 18907−18913.
(64) Grinis, L.; Kotlyar, S.; Ruehle, S.; Grinblat, J.; Zaban, A. *Adv. Funct. Mater.* **2010**, *20* (2), 282−288.
(65) Hodes, G. *J. Phys. Chem. C* **2008**, *112* (46), 17778−17787.
(66) Greenwald, S.; Ruhle, S.; Shalom, M.; Yahav, S.; Zaban, A. *Phys. Chem. Chem. Phys.* **2011**, *13* (43), 19302−19306.
(67) Bisquert, J.; Zaban, A.; Greenshtein, M.; Mora-Sero, I. *J. Am. Chem. Soc.* **2004**, *126* (41), 13550−13559.